Intelligent sensors using computationally efficient Chebyshev neural networks

Juhola, M.; Patra, Jagdish Chandra; Meher, Pramod Kumar

2008

Patra, J. C., Juhola, M., & Meher, P. K. (2008). Intelligent sensors using computationally efficient Chebyshev neural networks. IET Science, Measurement & Technology, 2(2), 68-75.

https://hdl.handle.net/10356/94242

https://doi.org/10.1049/iet-smt:20070061

Intelligent sensors using computationally efficient Chebyshev neural networks

J.C. Patra, M. Juhola and P.K. Meher
J.C. Patra and P.K. Meher are with the School of Computer Engineering, Nanyang Technological University, Singapore 639798, Singapore
M. Juhola is with the Department of Computer Sciences, University of Tempere, Finland
E-mail: aspatra@ntu.edu.sg

ABSRACT

Intelligent signal processing techniques are required for auto-calibration of sensors, and to take care of nonlinearity compensation and mitigation of the undesirable effects of environmental parameters on sensor output. This is required for accurate and reliable readout of the measurand, especially when the sensor is operating in harsh operating conditions. A novel computationally efficient Chebyshev neural network (CNN) model that effectively compensates for such non-idealities, linearises and calibrates automatically is proposed. By taking an example of a capacitive pressure sensor, through extensive simulation studies it is shown that performance of the CNN-based sensor model is similar to that of a multilayer perceptron-based model, but the former has much lower computational requirement. The CNN model is capable of producing pressure readout with a full-scale error of only ±1.0% over a wide operating range of -50 to 200 ℃.

1. INTRODUCTION

We begin by quoting Betts [1]: 'Chances are, your health and happiness rely on sensors, those ubiquitous little devices that tell us if a fridge is too cold, a nuclear reactor's safety systems are operating, or a factory production line is processing components correctly. But sensors have a dirty little secret: it's all too easy for them be in perfect working order, reporting all is well when, in fact, your milk is turning into a frozen block, the reactor's safety system is impotent, and that factory has filled a warehouse with useless and possibly dangerous products'.

Sensors of various kinds are widely used to measure temperature, pressure, flow, humidity and so on, in industrial processes, automobiles, robotics, avionics and other systems to monitor and control system behaviour. In addition, precise, accurate and low-power sensors are also required in the recently emerging wireless sensor networks to be used in intelligent homes, habitat monitoring and war-field applications. Therefore it is highly important that the sensor's output readout truly represents the physical quantity for which the sensor is designed.

Usually, all the sensors exhibit some nonlinear response characteristics. Moreover, the sensor characteristics are influenced by the environmental conditions in which it operates. For example, consider a capacitive pressure sensor (CPS) fixed in a car, an aeroplane engine or an oil drill. The sensor's output depends not only on its primary input, that is, the pressure, but also on the operating conditions, for example, temperature and humidity, because of the geometry of the sensor and property of the sensing material used. For example, the output voltage representing the applied pressure at 25 ℃ is not the same as that at 150 ℃. Another associated problem is that the dependence of the sensor response characteristics on the disturbing parameters may not be

linear. This further complicates the calibration of the sensor in order to obtain an accurate, precise and reliable readout.

The digital technology revolution has transformed the design of the industrial sensors. An embedded processor in a sensor can perform various functions, for example, compensation for temperature, in addition to sensing, control and communication functionalities [2]. In order to obtain an accurate and precise readout from a sensor, the adverse effects of the environmental parameters and non-linear characteristics are required to be suitably compensated for. In this direction, several iterative and non-iterative signal processing techniques have been proposed [3–11]. These techniques provide partial solutions to the complex problem under the assumptions that the variation in environmental parameters is small and that the influence of environmental parameters on the sensor characteristics is linear. Further, these solutions are not adequate for high-precision applications, because an exact mathematical model of a sensor showing the relationship between the measurand and its response and sensor's dependency on the environmental parameters is not available.

It has been shown that neural network (NN)-based approximations to measurement data perform better than those of classical methods, for example, interpolation and least mean square regression [12–16]. Application of NNs with superior performance for nonlinearity estimation in pressure sensor [17], compensation for environmental dependency and nonlinearities of sensor characteristics in pressure sensors [18–20] has been reported. Some other related successful applications of NNs in instrumentation and measurement may be found in [21–33].

Linearisation of sensor characteristics is another important issue as it makes sensor calibration easy. However, obtaining an exact linear characteristic is not an easy task, especially when the capacitive sensor is operated in harsh operating conditions with a wide variation in environmental parameters. The task becomes more complex when the disturbing parameters (e.g. temperature) influence the sensor characteristics nonlinearly. In this direction, a linearization technique using a simple multilayer perceptron (MLP) for a temperature sensor (a negative temperature coefficient resistor) has been reported [34], where a linearisation of 0.5% was obtained, for a small operating range of 60 ℃. Besides, the effect of disturbing environmental parameters was not considered in [34].

Most of the NN approaches, suggested so far for this application, are based on MLP. One major drawback of the MLP-based network is that it is computationally intensive and therefore involves a long time for training. In this article, we present a novel Chebyshev NN (CNN) that is computationally more efficient because of its single-layer architecture. The input signals first undergo a nonlinear transformation using Chebyschev polynomials and then applied to a single-layer NN. Recently, we have shown that CNN is capable of identifying complex dynamical systems quite effectively [35]. The performance of a CNN-based CPS model with preliminary results has been reported in [36]. In this article, we have shown, by taking an example of a CPS, that the performance of the CNN-based model is similar to that of the MLP-based model; however, the former takes less time for training. Through extensive computer simulations for three forms of nonlinear dependencies, we have shown that the maximum full-scale (FS) error remains within ±1% under operating temperature ranging from -50 to 200 ℃.

2. CPS AND SWITCHED CAPACITOR INTERFACE

A CPS senses the applied pressure in the form of elastic deflection of its diaphragm. The capacitance of the CPS resulting from the applied pressure P is given in terms of normalised pressure P_N by [5]

$$C(P_N) = C_0 + \Delta C(P_N) \quad (1)$$

where $P_N = P/P_{max}$, C_0 is the offset capacitance, that is, the zero-pressure capacitance, $\Delta C(P_N)$ the change in the capacitance because of applied pressure and P_{max} the maximum allowed pressure. The change in the capacitance $\Delta C(P_N)$ is given by [5]

$$\Delta C(P_N) = C_0 \cdot P_N \frac{1-\tau}{1-P_N} \quad (2)$$

where τ is a sensitivity parameter that depends on the physical geometry and material properties of the CPS.

Since the CPS response characteristics, that is, its capacitance, depend on the applied pressure as well as on the environmental temperature, using (1), the capacitance of the CPS at any pressure P and temperature T may be defined as

$$C(P_N, T_N) = C_0(T_0) f_1(T_N) + \Delta C(P_N, T_0) f_2(T_N) \quad (3)$$

where the normalised temperature T_N = (T–T_0)/($T_{max} - T_{min}$) and T_0, T_{min} and T_{max} denote the reference room temperature, the minimum and the maximum allowed operating temperatures, respectively. The offset capacitance at T_0 is denoted by $C_0(T_0)$. The functions $f_1(T_N)$ and $f_2(T_N)$ in (3) determine the influence of the temperature on the sensor characteristics and are given by

$$f_i(T_N) = 1 + \kappa_{i1} T_N + \kappa_{i2} T_N^2 + \kappa_{i3} T_N^3 \quad (4)$$

where i = 1 and 2. The coefficients, κ_{ij} {i = 1, 2 and j = 1, 2 and 3}, determine the extent of nonlinear influence of the temperature on the sensor characteristics. Note that for j = 2 and 3, when κ_{ij} = 0, the influence of the temperature on the CPS response characteristics is linear. Using (2), the change in capacitance $\Delta C(P_N, T_0)$ at T_0 is given by

$$\Delta C(P_N, T_0) = C_0(T_0) \cdot P_N \frac{1-\tau}{1-P_N} \quad (5)$$

The normalised capacitance C_N at any normalised operating temperature T_N may be expressed as

$$C_N = \frac{C(P_N, T_N)}{C_0(T_0)} \quad (6)$$

From (3) and (4), this may be rewritten as

$$C_N = f_1(T_N) + \gamma f_2(T_N) \quad (7)$$

where γ = P_N $(1-\tau)$/$(1-P_N)$. As γ = 0 when P_N is zero, the normalised zero-pressure capacitance (i.e. the normalised offset capacitance) at T_N is given by

$$C_{N0} = f_1(T_N) \quad (8)$$

A switched capacitor interface (SCI) for the CPS is shown in Fig. 1, in which the CPS is denoted as *C(P)*. The SCI output provides a voltage signal proportional to capacitance change in the CPS because of the applied pressure. The SCI output voltage is given by

$$V_0 = K \cdot C(P) \quad (9)$$

where $K = V_R/C_s$. By choosing proper values of the reference capacitor C_s and reference voltage V_R, the normalised SCI output V_N may be obtained such that

$$V_N = C_N \quad (10)$$

It is important to note that the SCI output changes when the ambient temperature changes, even though the applied pressure is fixed, thus giving rise to wrong sensor readout.

3. MLP- and CNN-BASED CPS MODEL

Here we describe the MLP- and CNN-based CPS models used to mitigate the adverse effects of the environmental parameters and to linearise the sensor characteristics. As an exact mathematical model describing the sensor operating in a harsh environment is not available, the NN-based approach is found to be quite effective. Our objective is to obtain a linearised sensor readout that is independent of nonlinear sensor characteristics and nonlinear effect of the environmental temperature.

3.1 Multilayer perceptron

Fig. 2 shows a schematic diagram of an MLP NN used in our study. A two-layer MLP architecture is specified by {*I–J–K*}, which has *I* neurons in the input layer, *J* neurons in the hidden layer and *K* neurons in the output layer. The MLP is trained using the popular backpropagation (BP) learning algorithm [37]. Let *y(k)* be the output of the MLP for a training input *x(k)*, and *d(k)* be the desired output, at *k*th instant. The error at the output layer is found to be *e(k)= d(k) – y(k).* The weight updating procedure using this error is repeated until the mean square error of the network approaches a pre-specified minimum value.

3.2 Chebyshev neural network

The structure of a CNN is depicted in Fig. 3. It consists of a functional expansion block and a single-layer perceptron network. The main purpose of the functional expansion block is to increase the dimension of the input pattern so as to enhance its representation in a higher-dimensional space. This enhanced pattern is then used for modelling of the sensor. Let us denote an *m*-dimensional input pattern vector at the *k*th instant by

$$X_k = [x_1(k), x_2(k), \ldots, x_m(k)] \quad (11)$$

Each element of the input vector is expanded into several terms using the Chebyshev polynomials. The Chebyshev polynomials are a set of orthogonal polynomials obtained as the solution to the Chebyshev differential equation. The *n*th-order Chebyhev polynomial is denoted by $T_n(x)$, where $-1 < x < 1$. The first few Chebyshev polynomials are given by

$$T_0(x) = 1$$
$$T_1(x) = x$$
$$T_2(x) = 2x^2 - 1 \quad (12)$$
$$T_3(x) = 4x^3 - 3x$$
$$T_4(x) = 8x^4 - 8x^2 + 1$$

The higher-order Chebyshev polynomials may be generated using a recursive formula given by

$$T_{n+1}(x) = 2xT_n(x) - T_{n-1}(x) \quad (13)$$

Thus, using the Chebyshev polynomials, an *m*-dimensional input pattern is enhanced into an *n*-dimensional *(n>m)* expanded pattern, which is then applied to a single-layer perceptron. In the CNN schematic shown in Fig. 3, $m = 2$ and $n = 9$ have been chosen. In addition, a few cross-product terms are also included in the expanded pattern to improve the original pattern representation in the expanded pattern space. The advantage of CNN over MLP is that the Chebyshev polynomials are computationally more efficient and take much less time to train when compared with the MLP network.

3.3 NN-based sensor model

A schematic diagram of the NN-based CPS model is shown in Fig. 4. The ambient temperature and the SCI output are the inputs to the NN. Appropriate scale factors are used to keep these values within ±1.0. The desired output is the linearised normalised voltage.

During the training phase, an input pattern from the training set is applied to the NN and its weights are updated using the BP algorithm. At the end of the training, the final weights are stored in an EEPROM. During the second phase, that is, the test phase, the stored final weights are loaded into the MLP. An input pattern from the test set is applied to the NN model and its output is computed. If the NN output and the target output match closely, then it may be said that the NN model has learnt the sensor characteristics satisfactorily.

To illustrate the effectiveness of the NN model for mitigating the nonlinear dependency of temperature on sensor characteristics, three different forms of nonlinear functions denoted by NL1, NL2 and NL3 have been selected. A linear function denoted by NL0 is also used for comparison purposes. These nonlinear functions are generated by using a different set of coefficients κ_{ij} in (4). In this study, the temperature information is assumed to be available. This can be obtained by using another temperature sensor. In this article, we have used two different NNs, that is, an MLP and a CNN to model the sensor and compare their performance.

3.4 Computational complexity

Here we present a comparison of computational complexity between MLP and CNN, where both the NNs are trained by the BP algorithm. Let us consider a two-layer MLP structure specified by *I, J* and *K* nodes (excluding the bias units) in the input, the hidden and the output layers, respectively. The CNN has *D* input nodes and *K* output nodes. Three basic computations, that is, addition, multiplication and computation of tanh(.), are involved for updating weights of

the NNs. For the MLP, the increased computation burden is due to the error propagation for the calculation of square-error derivative of each node in the hidden layer. In one iteration, all the computations in the network take place in three phases: (i) forward calculation to find the activation value of all nodes of the entire network; (ii) back error propagation for the calculation of square-error derivatives and (iii) updating the weights of the whole network.

The total number of weights to be updated in one iteration in the two-layer MLP is $J(I + 1) + K (J + 1)$, whereas in the case of CNN, it is $K(D + 1)$. It may be seen from Table 1 that as the hidden layer does not exist in the CNN, the computational complexity of CNN is much lower than the MLP structure.

4 .SIMULATION STUDIES

We carried out extensive simulation studies for the performance evaluation of the proposed MLP- and CNN-based CPS models.

4.1 Preparation of data sets

All the parameters of the CPS, such as the ambient temperature, the applied pressure and the SCI output voltage, used in the simulation study were suitably normalised to keep their values within ±1.0. The SCI output voltage (V_N) was recorded at the reference temperature (T_0 =25 ℃) with different known values of normalised pressure (P_N) chosen between 0.0 and 0.6 at an interval of 0.05. Thus, these 13 pairs of data (P_N against V_N) constitute the response characteristics of the CPS (the data set at T_0). To study the influence of temperature on the CPS characteristics, three forms of nonlinear functions NL1, NL2 and NL3 and a linear form NL0 were generated using (4) and selecting proper values of κ_{ij}. The selected values of the κ_{ij} are tabulated in Table 2. These values were selected randomly to provide different types of nonlinearities.

With the knowledge of the data set at the reference temperature and the chosen values of κ_{ij}, the response characteristics of the CPS for a specific ambient temperature were generated using (4). For temperature ranging from -50 to 200 ℃, at an increment of 10 ℃, 26 such data sets, each containing 13 data pairs, were generated using (4). These data sets were then divided into two groups: the training set and the test set. The training set, used for training the NNs, consists of only five data sets corresponding to -50, 10, 70, 130 and 190 ℃, and the remaining 21 data sets were used as the test set.

The sensor characteristics (the upper curves) for the four forms of dependencies (NL0, NL1, NL2 and NL3) at different temperatures and the desired linear response (bottom straight line) are plotted in Fig. 5. It can be seen that the response characteristics of the sensor change nonlinearly over the temperature range. Besides, the change in the response characteristics differs substantially for different forms of nonlinear dependencies. However, it is important to note that, in order to have accurate and precise readout, the sensor should provide linear response characteristics in spite of changes in ambient temperature and nonlinear temperature dependency.

4.2 Training and testing of MLP and CNN

A two-layer MLP with {2–5–1} architecture was chosen in this modelling problem (Fig. 4). Thus, the number of nodes including the bias units in the input, hidden and the output layers is 3,

6 and 1, respectively. This MLP contains only 21 weights. The two inputs to the MLP were the normalised temperature (T_N) and the normalised SCI output voltage (V_N). The linear normalised voltage V_{Lin} was used as the target output for the MLP.

Initially, all the weights of the MLP were set to random values within ±0.5. During training, one data set out of the five was chosen randomly. The learning parameter α and the momentum factor β used in the BP algorithm were selected as 0.3 and 0.5, respectively. Completion of weight adaptation for the 13 data pairs of all the five training sets constitutes one iteration. For effective learning, 50 000 iterations were made to train the MLP model. To improve the learning process of the NNs, the learning parameter

$$\alpha_i = \alpha_{i-1}\left(1 - \frac{i}{N_t}\right) \qquad (14)$$

where i is the current iteration number and N_t is the total number of iterations used (N_t = 50 000 in this case). Using a Pentium 1.10 GHz machine, it took 12 s to train the MLP.

In the case of CNN, the following parameters were selected. The two-dimensional input pattern was expanded to a 12-dimensional pattern by using Chebyshev polynomials (12). Here, both the T_N and P_N were expanded by fourth-order Chebyshev polynomials. In addition, four cross-product terms were included to make a 12-dimensional expanded pattern. Both the learning parameter and the momentum parameter were chosen as 0.5. The training was continued for 50 000 iterations. For the five training sets, it took only 6.0 s to train the CNN, which is half of the time taken by an MLP. Note that the number of weights in the MLP and CNN was 21 and 12, respectively.

5. RESULTS AND DISCUSSIONS

On the basis of the results of the simulation studies, we provide here the performance evaluation of the MLP- and the CNN-based models for linearisation, auto-calibration and auto-compensation for the CPS.

5.1 Linear response characteristics

The NN-based models were able to produce linear response characteristics. The results obtained through the simulation for the linear (NL0) and one nonlinear (NL1) temperature dependency are provided in Fig. 6, for the MLP- and the CNN-based sensor models. The response characteristics at different temperatures (-40, 100, 150, and 200 ℃) for both NL0 and NL1 are almost linear, in the case of both the networks. It may be noted that during the training phase, the NNs were not exposed to the sensor characteristics for these temperatures. The upper curve, which represents the sensor characteristics (SCI output) at the reference temperature (T_0 = 25 ℃), is shown for the purpose of comparison. Similar observations were made for the nonlinear temperature dependencies NL2 and NL3 (data not shown). Thus, both the MLP and CNN are able to transfer SCI output voltage from the actual to the linearised values quite effectively over a wide range of temperature and for the linear as well as the three nonlinear dependencies.

5.2 FS error

The FS percent error is defined as

$$\text{FS error} = 100 \text{ x } \frac{y_{\text{lin}} - y_{\text{est}}}{y_{\text{fs}}} \qquad (15)$$

where y_{lin} and y_{est} denote the desired linearised sensor readout and the NN model output, respectively. As all the values are normalised to ±1.0, the y_{fs} is selected as 1.0. The FS percent error in the estimation of normalised response at different temperatures for the NL2 and NL3 at specific values of P_N is plotted in Fig. 7 for the MLP- and the CNN-based models. It may be seen that the FS error remains within ±1.0% for a wide range of temperature from -50 to 200 ℃ for NL2 and NL3. However, only at 200 ℃, the FS error is 1.5% for NL2.

The FS errors between the estimated and desired responses at different values of temperature over the entire range of applied pressure are shown in Fig. 8. Here, again the FS error remains within ±1.0%, except in the case of temperature at 200 ℃ when P_N = 0.0. Similar observations were made for the linear (NL0) and nonlinear (NL1) temperature dependencies (data not shown).

From Figs. 7 and 8, one can see that the FS error remains within ±1.0% for the linear (NL0) and the three nonlinear (NL1, NL2 and NL3) dependencies for both the MLP- and CNN-based models. However, in the case of an MLP-based model, only at 200 ℃, for lower values of P_N, the FS error exceeds 1.0%, but remains within 1.5%. Whereas in the case of a CNN-based model, the FS error becomes 1.5% only at 200 ℃ when P_N = 0.0. This shows the superiority of the CNN-based model over the MLP. It may be noted that the data sets used for training the two networks were data sets corresponding to only five temperatures (-50, 10, 70, 130 and 190 ℃). As 200 ℃ is beyond this range of training data, the FS error is slightly more when compared with those at other values of temperature.

6. CONCLUSIONS

Smart sensors should be capable of providing accurate readout, auto-calibration and auto-compensation for the nonlinear influence of the environmental parameters on its characteristics. We have proposed a novel computationally efficient CNN-based technique to incorporate these capabilities in a CPS operating in a harsh environment in which the temperature can have wide variations.

We have shown the effectiveness of the model in different forms of nonlinear influence of the ambient temperature on the pressure sensor characteristics. We have seen that the sensor characteristics change widely when the environmental temperature changes over a wide range from -50 to 200 ℃. Additionally, the surrounding temperature influences the sensor characteristics nonlinearly. In spite of these facts, the MLP- and the CNN-based models are able to provide an accurate estimate of the applied pressure. From the above-mentioned findings, it may be concluded that the performance of both the NN models for linearisation, and auto-compensation is quite satisfactory for linear and nonlinear forms of temperature dependencies. The maximum FS error of the NN models for the estimation of pressure remains within ±1.0% for the linear and the three forms of nonlinear interactions.

The proposed CNN-based model is found to be computationally more efficient than the MLP network as the former is a single-layer network. We have also shown that the CNN-based model performs better than the MLP-based model in terms of FS error and linearisation of sensor

characteristics. Such NN-based models may be applied to other types of sensors to infuse intelligence in terms of auto-calibration and to mitigate the nonlinear dependency of their response characteristics on the environmental parameters. The proposed CPS model may be used for online applications. Once the CNN is trained, it captures the sensor characteristics and behaviour of the nonlinear environment and therefore is capable of producing linearised sensor output. In addition, it is possible to train the CNN in unknown operating conditions with a known set of training data.

7. ACKNOWLEDGEMENTS

The authors wish to acknowledge with thanks the Nokia Foundation, Finland, for providing the Research Fellowship to the first author to carry out major part this research at the University of Tampere, Finland, during May–July 2007. The authors also wish to offer their sincere thanks to the anonymous reviewers whose valuable comments and suggestions helped to enhance the quality of this article.

8. REFERENCES

[1] Betts, B.: 'Smart sensors', *IEEE Spectr.*, 2006, **43**, (4), pp. 50–53

[2] Henry, M.: 'Plant asset management via intelligent sensors', *IEE Comput. Control Eng. J.*, 2000, **11**, (3), pp. 211–213

[3] Van der Goes, F.M.L., and Meijer, G.C.M.: 'A simple accurate bridge–transducer interface with continuous autocalibration', *IEEE Trans. Instrum. Meas.*, 1997, **46**, (3), pp. 704–710

[4] Li, X., and Meijer, G.C.: 'An accurate interface for capacitive sensors', *IEEE Trans. Instrum. Meas.*, 2002, **51**, (5), pp. 935–939

[5] Yamada, M., Takebayashi, T., Notoyama, S.-I., and Watanabe, K.: 'A switched-capacitor interface for capacitive pressure sensors', *IEEE Trans. Instrum. Meas.*, 1992, **41**, (1), pp. 81–86

[6] Yamada, M., and Watanabe, S.-I.: 'A capacitive pressure sensor interface using oversampling Δ– ∑demodulation techniques', *IEEE Trans. Instrum. Meas*., 1997, **46**, (1), pp. 3–7

[7] Hille, P., Hohler, R., and Strack, H.: 'A linearization and compensation method for integrated sensors', *Sens. Actuators-B*, 1994, **44**, pp. 95–102

[8] Sabatini, A.M.: 'A digital signal-processing technique for compensating ultrasonic sensors', *IEEE Trans. Instrum. Meas*., 1995, **46**, (4), pp. 869–874

[9] Maric, I.: 'Automatic digital correction of measurement data based on M-point autocalibration and inverse polynomial approximation', *IEEE Trans. Indus. Electron*., 1988, **35**, (2), pp. 317–322

[10] Lyahou, K.F., Van der Horn, G., and Huijsing, J.H.: 'A noniterative polynomial 2-D calibration method implemented in a microcontroller', *IEEE Trans. Instrum. Meas*., 1997, **46**, (4), pp. 752–757

[11] Li, X., Meijer, G.C., and De Jong, G.W.: 'A microcontroller-based self-calibration technique for a smart capacitance angular-position sensor', *IEEE Trans. Instrum. Meas*., 1997, **46**, (4), pp. 888–892

[12] Pau, L.F., and Johansen, F.S.: 'Neural network signal understanding for instrumentation', *IEEE Trans. Instrum. Meas*., 1990, **39**, (4), pp. 558–564

[13] Daponte, P., and Grimaldi, D.: 'Artificial neural networks in measurements', *Measurement*, 1998, **23**, pp. 93–115

[14] Dias Pereira, J.M., Silva Girao, P.M.B., and Postolache, O.: 'Fitting transducer characteristics to measured data', *IEEE Instrum. Meas. Mag*., 2001, **4**, (4), pp. 26–39

[15] Morawski, R.Z.: 'Digital signal processing in measurement microsystems', *IEEE Instrum. Meas. Mag.*, 2004, **7**, (2), pp. 43–50

[16] Singh, A.P., Kumar, S., and Kamal, T.S.: 'Fitting transducer characteristics to measured data using a virtual curve tracer', *Sens. Actuators-A*, 2004, **111**, pp. 145–153

[17] Patra, J.C., Panda, G., and Baliarsingh, R.: 'Artificial neural network-based nonlinearity estimation of pressure sensors', *IEEE Trans. Instrum. Meas.*, 1994, **43**, (6), pp. 874–881

[18] Patra, J.C., Kot, A.C., and Panda, G.: 'An intelligent pressure sensor using neural networks', *IEEE Trans. Instrum. Meas*., 2000, **49**, (4), pp. 829–834

[19] Patra, J.C., Van den Bos, A., and Kot, A.C.: 'An NN-based smart capacitive pressure sensor in dynamic environment', *Sens. Actuators-B*, 2000, **86**, pp. 26–38

[20] Patra, J.C., Ang, E.L., Chaudhari, N.S., and Das, A.: 'Neural-network-based smart sensor framework operating in a harsh environment', *J. Appl. Signal Process.,* 2005, **4**, pp. 558–574
[21] Dias Pereira, J.M., Postolache, O., and Girao, P.M.B.: 'A temperature compensated system for magnetic field measurements based on artificial neural networks', *IEEE Trans. Instrum. Meas.,* 1998, **47**, (2), pp. 494–498
[22] Carullo, A., Ferraris, F., Graziani, S., Grimaldi, U., and Parvis, M.: 'Ultrasonic distance sensor improvement using a two-level neural networks', *IEEE Trans. Instrum. Meas.,* 1996, **45**, pp. 677–682
[23] Arpaia, P., Daponte, P., Grimaldi, D., and Michaeli, L.: 'ANN-based error reduction for experimentally modeled sensors', *IEEE Trans. Instrum. Meas.,* 2002, **51**, (1), pp. 23–30
[24] Singh, A.P., Kumar, S., and Kamal, T.S.: 'Development of ANN-based virtual fault detector for Wheatstone bridge-oriented transducer', *IEEE Sens. J.,* 2005, **5**, pp. 1043–1049
[25] Singh, A.P., Kumar, S., and Kamal, T.S.: 'Virtual compensator for correcting the disturbing variable effect in transducers', *Sens. Actuators-A,* 2004, **116**, pp. 1–9
[26] Khan, A.M.: 'Intelligent infrastructure-based queue-end warning system for avoiding rear impacts', *IET Intell. Transp. Syst.,* 2007, **1**, (2), pp. 138–143
[27] Petra, I., Holding, D.J., Ma, X., Brett, P.N., and Blow, K.J.: 'Fast and accurate tactile sense feedback estimation for innovative flexible digit for clinical applications', *Electron. Lett,* 2006, **42**, (14), pp. 790–792
[28] Yates, J.W.T., Gardener, J.W., Chappell, M.J., and Dow, C.S.: 'Identification of bacterial pathogens using quadrupole mass spectrometer data and radial basis function neural networks', *IEE Proc., Sci. Meas. Technol.,* 2005, **152**, (3), pp. 97–102
[29] Mukhopadhyay, S.C.: 'Quality inspection of electroplated materials using planar type micro-magnetic sensors with post-processing from neural network model', *IEE Proc., Sci. Meas. Technol.,* 2002, **149**, (4), pp. 165–171
[30] Dowdeswell, R.M., and Payne, P.A.: 'Odour measurement using conducting polymer gas sensors and an artificial neural network decision system', *IEE Eng. Sci. Edu. J.,* 1999, **8**, (3), pp. 129–134
[31] Yasin, S.M.T.A., and White, N.M.: 'Application of artificial neural networks to intelligent weighing systems', *IEE Proc., Sci. Meas. Technol.,* 1999, **146**, (6), pp. 265–269
[32] Hines, E.L., Llobet, E., and Gardener, J.W.: 'Electronic noses: a review of signal processing techniques', *IEE Proc., Circuits Dev. Syst.,* 1999, **146**, (6), pp. 297–310
[33] Fotis, G.P., Ekonomou, L., Maris, T.I., and Liatsis, P.: 'Development of an artificial neural network software tool for the assessment of the electromagnetic field radiating by electrostatic discharges', *IET Sci., Meas. Technol.,* 2007, **1**, (5), pp. 261–269
[34] Medrano-Marques, N.J., and Martin-del-Brio, B.: 'Sensor linearization with neural networks', *IEEE Trans. Indus. Electron.,* 2001, **48**, (6), pp. 1288–1290
[35] Patra, J.C., and Kot, A.C.: 'Nonlinear dynamic system identification using Chebyshev functional link artificial neural networks', *IEEE Trans. Syst., Man Cybern., Part B: Cybern.,* 2002, **32**, (3), pp. 1–7
[36] Patra, J.C., and Juhola, M.: 'Intelligent sensors using Chebyshev neural networks'. *Proc. Intl. Conf. Sensing Technology,* Palmerston North, New Zealand, November 2007, pp. 420–425

[37] Haykin, S.: ‘Neural networks’ (Maxwell MacMillan, Ontario, Canada, 1994)

List of Tables

List of Figures

Operation	MLP$(I-J-K)$	CNN$(D-K)$
addition	$4IJ+3JK$	$3K(D+1)$
multiplication	$6J(I+K)$	$6K(D+1)$
tanh()	$J+K$	K

Table 1

NL form	κ_{11}	κ_{12}	κ_{13}	κ_{21}	κ_{22}	κ_{23}
NL0	0.10	0.00	0.00	0.20	0.00	0.00
NL1	0.25	−0.25	0.10	0.20	−0.40	0.40
NL2	0.30	0.10	−0.30	0.20	−0.20	−0.10
NL3	0.40	−0.15	−0.15	0.25	0.30	−0.60

Table 2

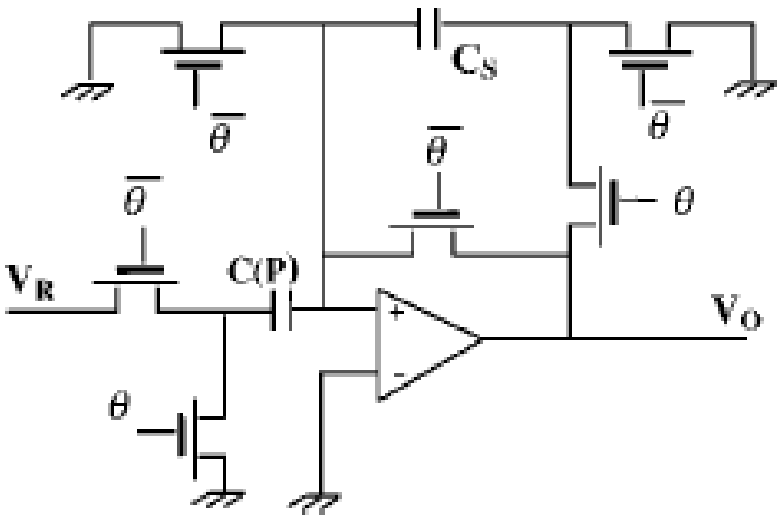
C_S
$\overline{\theta}$
$\overline{\theta}$
$\overline{\theta}$
θ
$\overline{\theta}$
V_R
C(P)
V_O
+
-
θ

Figure 1

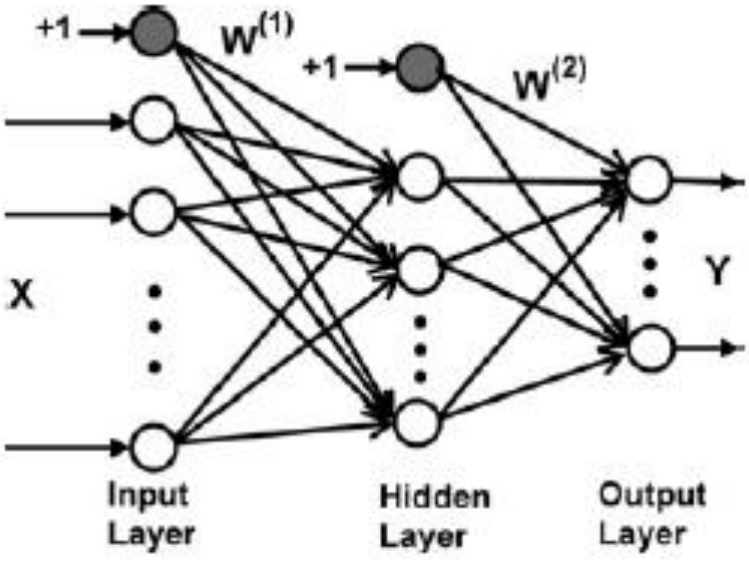

Figure 2

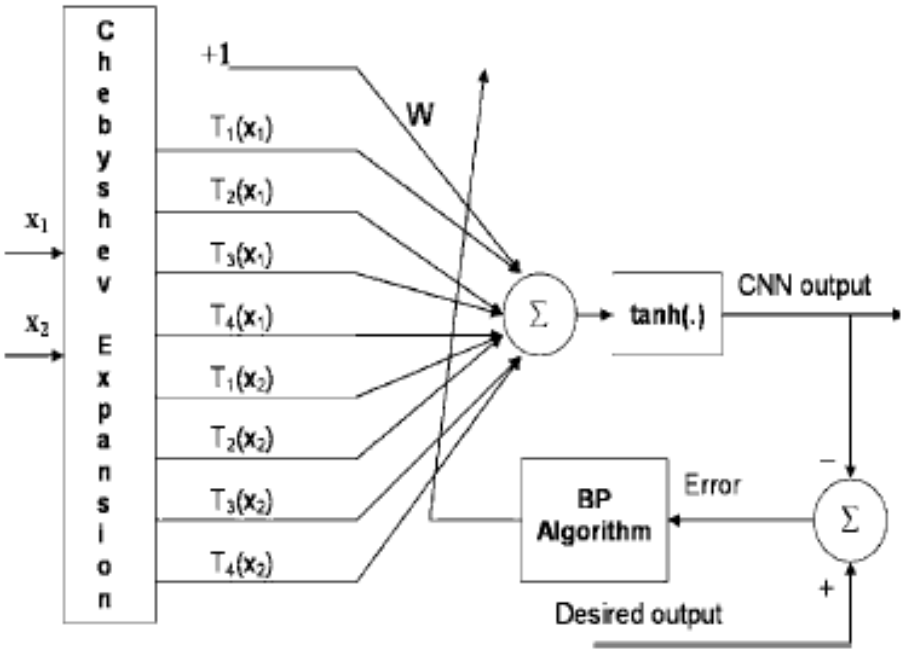
Chebyshev Expansion
x1
x2
+1
T1(x1)
T2(x1)
T3(x1)
T4(x1)
T1(x2)
T2(x2)
T3(x2)
T4(x2)
W
Σ
tanh(.)
CNN output
BP Algorithm
Error
Σ
−
+
Desired output

Figure 3

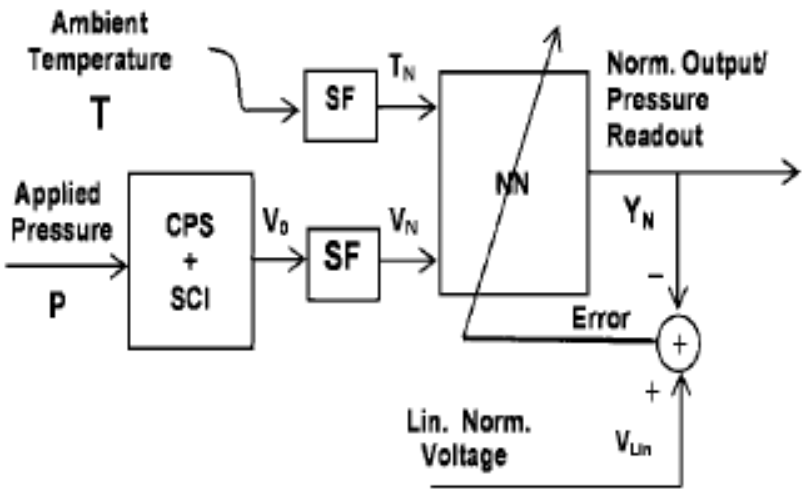
Ambient
Temperature
T
SF
T_N
NN
Norm. Output/
Pressure
Readout
Applied
Pressure
P
CPS
+
SCI
V_0
SF
V_N
Y_N
−
Error
+
+
Lin. Norm.
Voltage
V_{Lin}

Figure 4

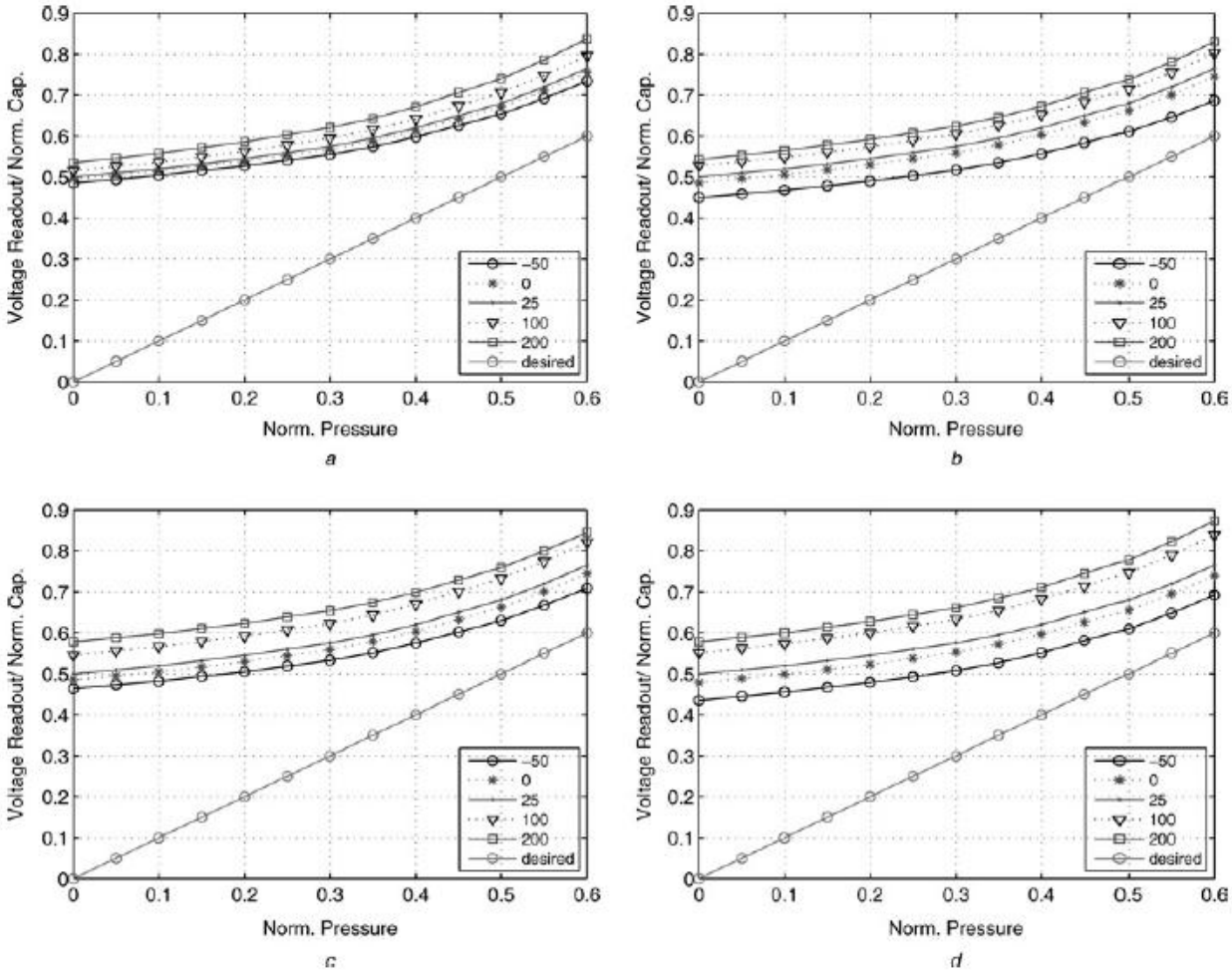
Voltage Readout/ Norm. Cap.
Norm. Pressure
−50
0
25
100
200
desired
a
b
c
d

Figure 5

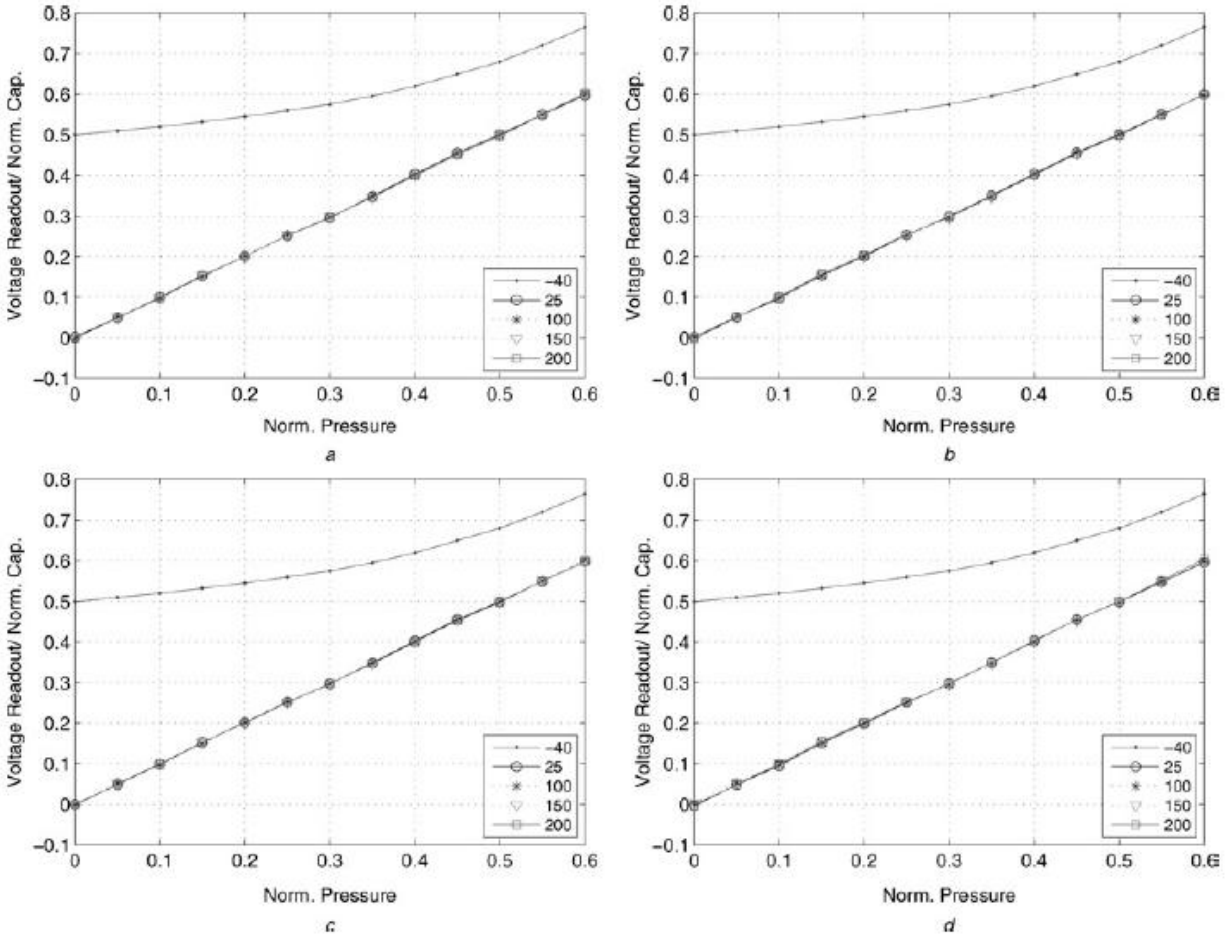
Voltage Readout/ Norm. Cap.
Norm. Pressure
−40
25
100
150
200
a
b
c
d

Figure 6

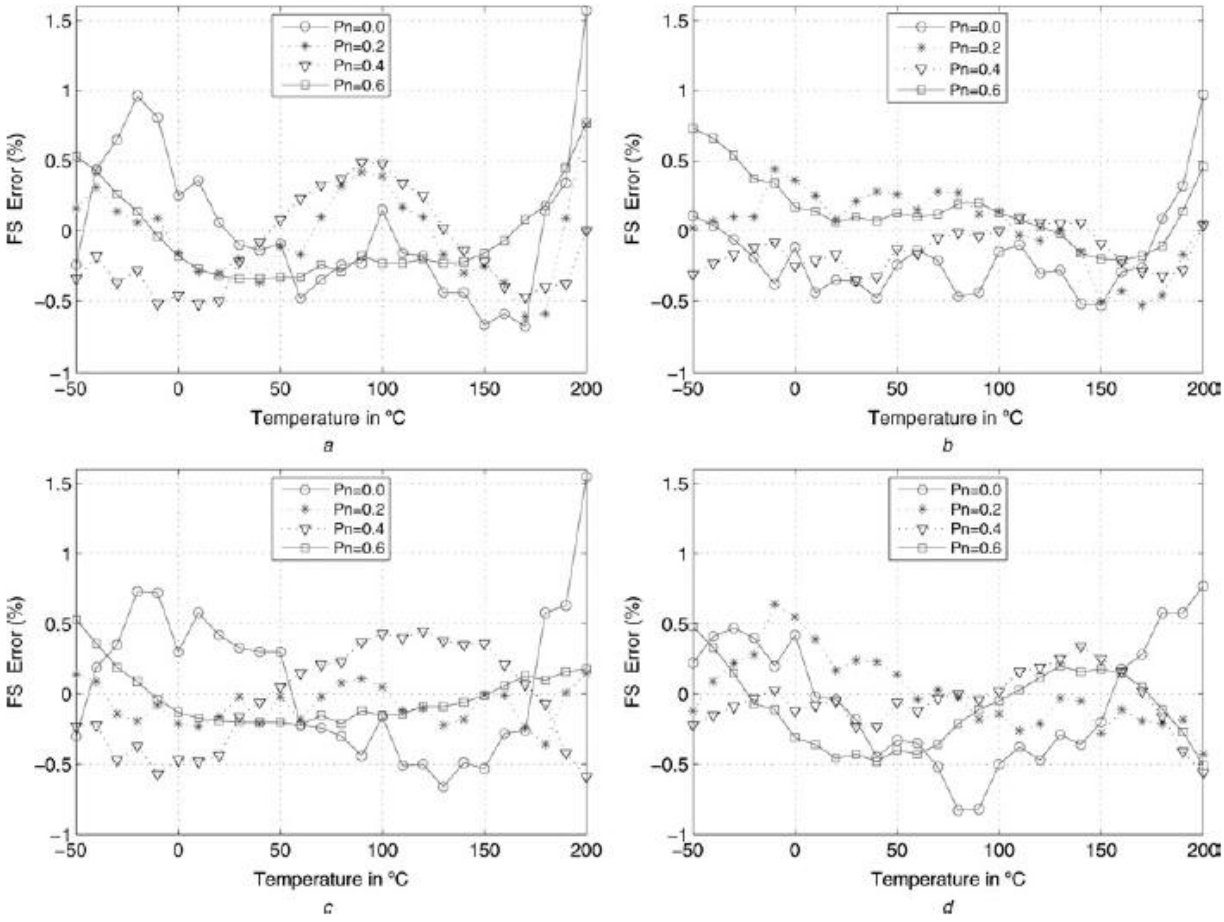

Figure 7

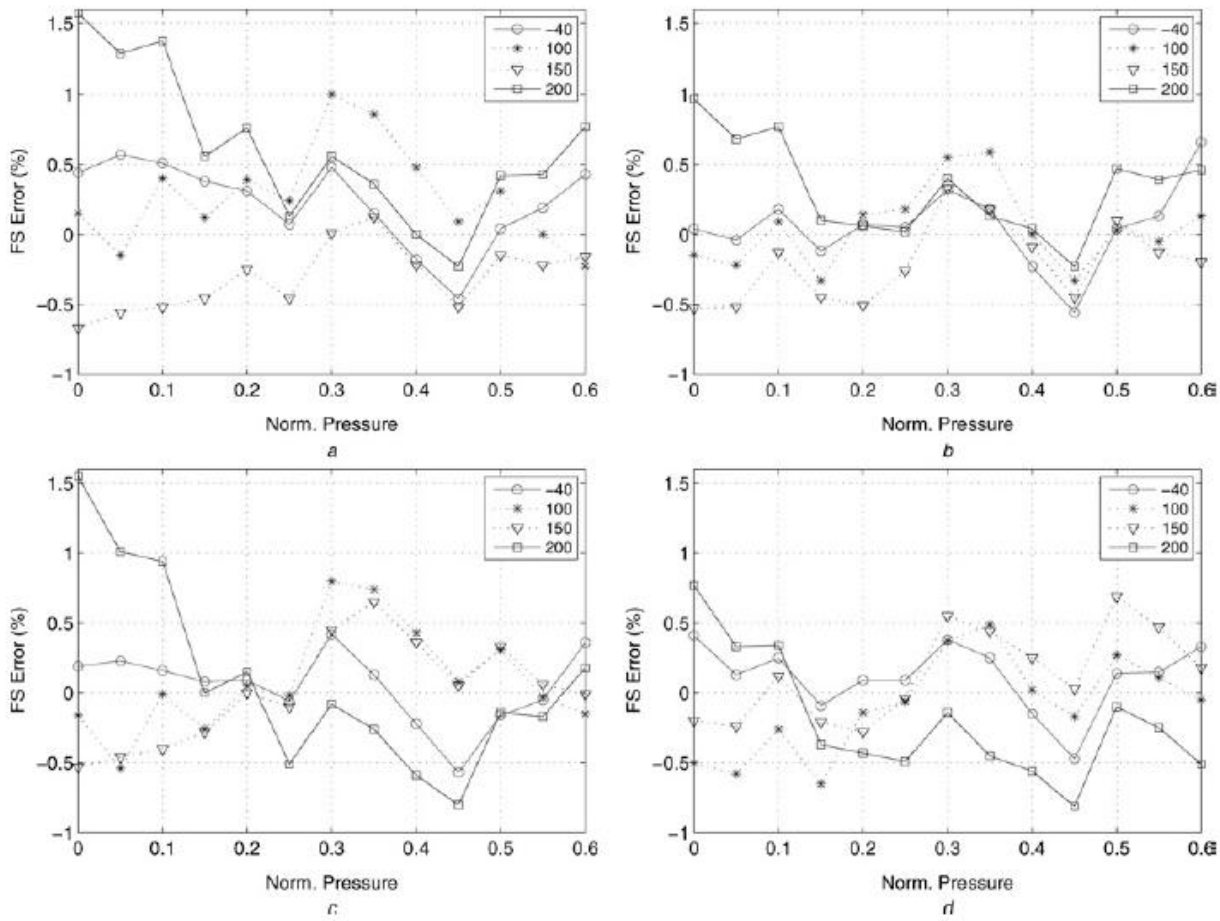

Figure 8